第 9 回地震時保有耐力法に基づく橋梁等構造の
耐震設計に関するシンポジウム講演論文集（2006 年 2 月）

THE INELASTIC BEHAVIOR OF H-SECTION STEEL BEAM-COLUMNS UNDER CYCLIC LATERAL LOADING

Xiang Ma[1], Tsutomu Usami[2], Hanbin Ge[3]

[1]Grad. Student, Dept. of Civil Engineering, Nagoya University (〒464-8603 Furo-cho Chikusa-ku, Nagoya)
[2]Professor, D. Sc., D. Eng., Dept. of Civil Engineering, Nagoya University (〒464-8603 Furo-cho Chikusa-ku, Nagoya)
[3]Associate Professor, D. Eng., Dept. of Civil Engineering, Nagoya University (〒464-8603 Furo-cho Chikusa-ku, Nagoya)

1. Introduction

H-section members are widely used in steel structures, and in many cases are designed to function as beam-columns undergoing both axial and lateral load. Complicated instability phenomena are associated with H-section members, which are characterized by the open section and a smaller bending rigidity about weak axis of the cross section. In addition to local buckling of the plate components, they are also known to be subject to lateral buckling. In areas with a high seismic hazard, the cyclic loading condition induced by earthquake effect should be given further attention. Extensive research has been conducted to investigate the behavior of H-section structural members with different emphases. Lee and Galambos[1] conducted experiments to monotonically bend beams until failure. They found beams with proper transverse bracing possess sufficient deformation capacity even after lateral buckling occurs, and local buckling is the ultimate cause of failure. Cyclic loading condition was implemented in tests on cantilever beams by Bertero and Popov[2] who concluded that local buckling of flanges, rather than low cycle fatigue, is of the utmost importance regarding the deformation capacity of H-section beams. Lee and Lee[3] found for short members, under monotonic as well as cyclic loading condition, the influence of local buckling is more serious when axial force is present. In cyclic pure bending experiments[4] on longer beams, lateral buckling was observed and was found to have driven the occurrence of local buckling. Other tests[5-7] of beam-columns subjected to combined axial and cyclic lateral forces evidenced both lateral and local buckling, and confirmed the effect of axial force and cyclic loading on the deterioration of their force bearing capacity. Though most of the characteristics of H-section structural members have been identified in previous research, the following aspects are still of particular interest:

(1) Most previous efforts were concentrated on loading about strong axis of the cross section. However, in the event of an earthquake, severe cyclic loading about the weak axis may also be encountered.

(2) Though the process of failure under monotonic loading has been well understood, an accurate description of the failure mechanism under cyclic loading, especially the influence of cyclic loading on development of local buckling, lateral buckling and their interaction, is not found.

(3) In addition to analysis of individual members or members with extreme dimensions, a comprehensive study of members with systematic variation in parameters such as slenderness ratio, width-to-thickness ratio of the flange and axial force ratio is needed to thoroughly understand their influence on the behavior of H-section members.

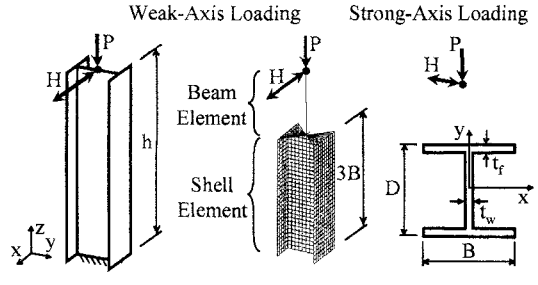

(a) Cantilever Column (b) FEM Model (c) Cross Section

Fig. 1 Analytical Model

By seeking answers to the questions stated above, the objective of the present research is to thoroughly investigate the inelastic behavior of H-section beam-columns with an emphasis in cyclic loading scope. Numerical method is employed so that a great number of analytical cases of interest can be included, which is hardly possible by means of experimental method. A cantilever H-section column which represents one half of a simply supported structural member is modeled by finite element method. In past research, the free end is often restrained to in-plane motions whereas in the present study it is left free to twist and deflect laterally in order to impose a more adverse condition for lateral buckling. Validity of the numerical model is confirmed through comparison with experimental results. Members with various dimensional and loading parameters are subjected to combined axial force and lateral loading, both about strong axis and weak axis. The results are summarized to elucidate the failure mechanisms, and the variation in failure modes induced by cyclic loading is highlighted.

2. Finite Element Modeling

The commercial software package ABAQUS 6.5 is employed to perform FEM analysis. To account for the local buckling behavior, a four-node doubly curved shell element (SR4) is used to model the cantilever column. Combined axial and horizontal

Table 1 Dimension and Loading Conditions of Tested Specimens

Specimen	D (mm)	B (mm)	t_f (mm)	t_w (mm)	P/P_y	h/r_x	h/r_y	Δ_a/Δ_{pc}	Plate	
									Flange	Web
A	100.4	100.1	4.49	3.24	0.0	17.2	29.9	5.0	4.5-A	3.2-A
B	135.6	100.2	6.61	3.13	0.3	16.9	39.3	5.0	6-C	3.2-B

Table 2 Material Properties of Tested Specimens

Plate	σ_y (MPa)	σ_u (MPa)	ε_u (%)	ε_{st} (%)	$\varepsilon_{st}/\varepsilon_y$	E/E_{st} (%)
3.2-A	316	442	27.3	1.15	7.5	1.61
3.2-B	288	368	26.1	1.98	14.1	1.05
4.5-A	324	472	29.8	1.39	8.8	1.76
6-C	312	438	27.9	2.08	13.7	1.58

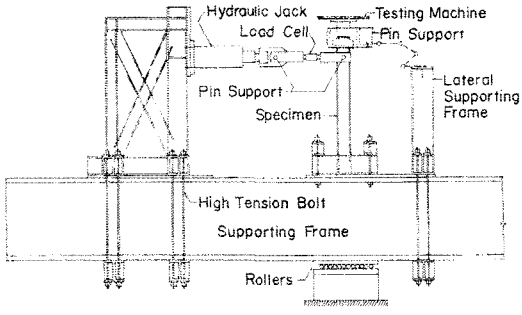

Fig. 2 Loading Arrangement

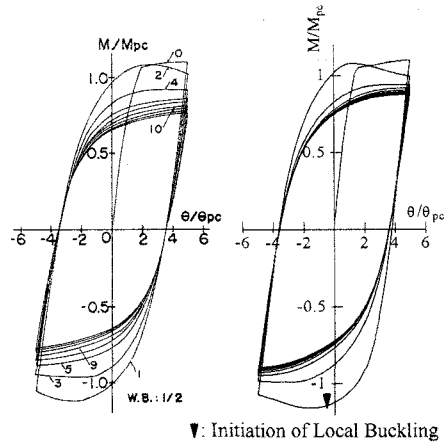

▼: Initiation of Local Buckling

(a) Specimen A

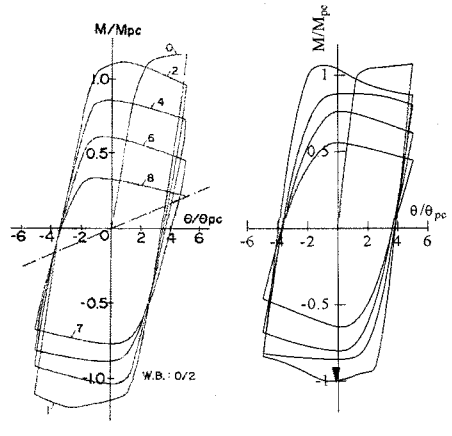

(b) Specimen B

Fig. 3 Comparison of M-θ Relations

loading is applied at its free tip (**Fig. 1 (a)** and **(b)**). When local buckling occurs, it is known that the buckle will form near the fixed end of the column where the largest axial strains concentrate. Thus only a certain length (L_{shell}) measured from the bottom is meshed by shell element to reduce calculation cost, while the remaining upper portion is modeled by a two-node three dimensional linear beam element (B31). A proper value of L_{shell} should be selected to ensure (1) the local buckling behavior is well represented; (2) the overall features including load-deflection relation, effect of uniform torsion and warping involved in lateral buckling are adequately embodied. The detailed mesh divisions and a proper L_{shell} are determined by try and error method. The mesh illustrated in **Fig. 1 (b)** is found to be sufficient to give reliable results.

As to modeling of steel material, expression of cyclic plastic hardening rule is very important when reversed loading is expected. There are two famous theories known as the kinematic hardening rule (KH) and the isotropic hardening rule (IH), each representing one typical expression, but also containing apparent approximation. A modified two-surface model (2SM) was developed by Shen et al.[8] which can account for both Bauschinger effect and varying strain hardening rate. To compare the effectiveness of KH, IH and 2SM, extensive numerical simulation[9] was conducted for box-section and pipe-section steel columns under axial and cyclic horizontal loading. By comparison with experimental results, 2SM was found to be superior over the other two in not only predicting the load-deflection relation, but also accurately reproducing the buckling deformation. Based on these findings, the 2SM is adopted in this research as the cyclic plastic hardening law.

3. Experimental Verification of the Finite Element Model

The experimental results of a previous research by Makino et al.[7], whose objects and loading condition similar with the present work, are used to verify the created numerical model. The loading arrangement of the experiment is shown in **Fig. 2**. The dimensional and loading parameters of the analyzed specimens are listed in Table 1. Indication of these parameters is illustrated in **Fig. 1**. Cyclic lateral loading was applied about the strong axis by alternating the horizontal displacement at the free end with a constant amplitude Δ_a. Δ_{pc} is calculated as follows: $\Delta_{pc}=\theta_{pc}h$, $\theta_{pc}=(M_{pc}h)/(\eta EI)$, $\eta=(z^2\sin z)/(\sin z-z\cos z)$, $z=\sqrt{(Ph^2/(EI))}$, where E: Young's Modulus; I: moment of inertia of the cross section; M_{pc}: plastic moment with axial force considered. Material properties are listed in Table 2. It is noted that the out-of-plane motions and twisting are restrained at the free end where loading is applied.

The numerical model was modified to be in accordance with the experimental setting. An initial global transverse geometric imperfection is assumed to seed the lateral deformation of the column. The shape of the imperfection is determined based on prediction of buckling eigenvalue analysis, with a maximum deflection of h/1000. Nondimensionalized M-θ relations obtained from the experiment and numerical analysis are shown in **Fig. 3**. It is observed for both specimens the results of the numerical analysis generally compare well with the experiments. The overall shapes of the hysteresis loops are alike. The deterioration of strength and unloading stiffness as cycling progresses are captured

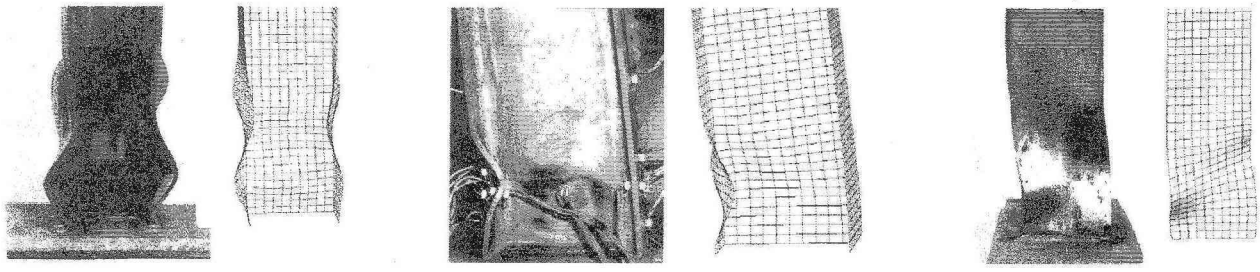

(a) (b) (c)

Fig. 4 Comparison of Buckling Deformation

Table 3 Geometrical Properties of Studied Cases [a]

Strong-axis Loading					Weak-axis Loading				
Case	$\bar{\lambda}_{strong}$	R_f	t_f (mm)	h (mm)	Case	$\bar{\lambda}_{weak}$	R_f	t_f (mm)	h (mm)
(1)	(2)	(3)	(4)	(5)	(6)	(7)	(8)	(9)	(10)
S02-40	0.2	0.40	28	1602	W02-40	0.2	0.40	28	966
S02-53	0.2	0.53	21	1600	W02-53	0.2	0.53	21	937
S02-69	0.2	0.69	16	1585	W02-69	0.2	0.69	16	903
S04-40	0.4	0.40	28	3203	W04-40	0.4	0.40	28	1933
S04-53	0.4	0.53	21	3199	W04-53	0.4	0.53	21	1873
S04-69	0.4	0.69	16	3171	W04-69	0.4	0.69	16	1806
S06-40	0.6	0.40	28	4805	W06-40	0.6	0.40	28	2899
S06-53	0.6	0.53	21	4799	W06-53	0.6	0.53	21	2810
S06-69	0.6	0.69	16	4756	W06-69	0.6	0.69	16	2709
S08-40	0.8	0.40	28	6406	W08-40	0.8	0.40	28	3865
S08-53	0.8	0.53	21	6399	W08-53	0.8	0.53	21	3747
S08-69	0.8	0.69	16	6341	W08-69	0.8	0.69	16	3612

[a] Constants: B=D=400 mm

Table 4 Material Properties of Steel SS400

Steel Type	σ_y (MPa)	E/E_{st}	$\varepsilon_{st}/\varepsilon_y$	E (GPa)	ξ	ν
SS400	235	40	10	205	0.06	0.3

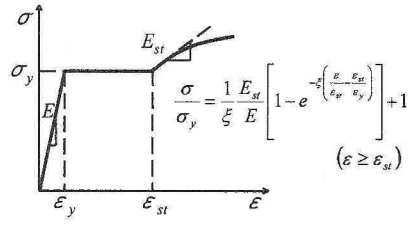

Fig. 5 Stress-strain Relation

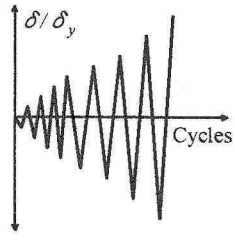

Fig. 6 Cyclic Loading Pattern

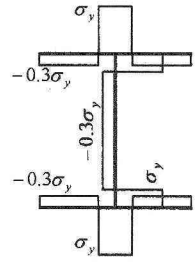

Fig. 7 Residual Stress Distribution

by the numerical analysis, though at a slower rate. In numerical simulation, initiation of local buckling is determined from visual observation, and indicated with an arrow in the hysteresis loops. Initial appearance of local buckling agrees with the experiment which reported that local buckling occurred in the loading route from loop 0 to loop 1.

Buckling deformations are compared in **Fig. 4**. From **Fig. 4 (a)** and **(b)** it can be seen the buckling shapes are quite similar, and number of buckling waves is the same. **Fig. 4 (c)** shows that numerical analysis yielded similar lateral deflection. Buckling deformation in analysis is smaller in scale with reference to experimental observations, which might be one of the reasons that attribute to the slower deterioration of strength and stiffness in analysis.

In general, the numerical model created in this research provided satisfactory prediction of load-deflection relation and buckling deformation. It is believed to be reliable for the objectives of the present research.

4. Results of Numerical Analysis

The numerical model is explained in the Finite Element Modeling section, and illustrated in **Fig. 1**. The free end of the analyzed cantilever column is subject to no restraint, therefore free to twist and deflect laterally. Deflection expressed by Eq. 1 is assumed about the weak axis as initial geometric imperfection to excite lateral buckling.

$$\omega_{0x} = \frac{h}{1000}\left[\sin\frac{\pi}{2h}(z+h)-1\right] \quad (1)$$

A listing of the studied columns is given in Table 3. The columns fall into two series, those loaded about the strong axis of cross section, and those about the weak axis. Slenderness ratio parameter $\bar{\lambda}$ and width-to-thickness ratio parameter of the flange R_f, defined by Eq. 2 and Eq. 3, are used to indicate the dimensional characteristics.

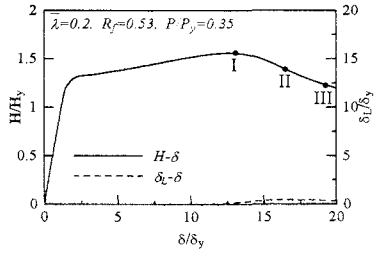

(a) Monotonic Loading

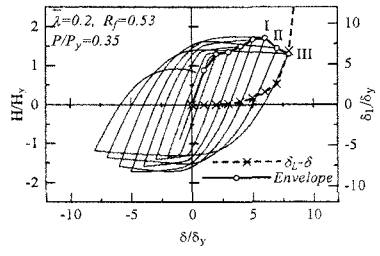

(b) Cyclic Loading

Fig. 8 Comparison of H-δ Curves for Short Members Loaded about Strong Axis

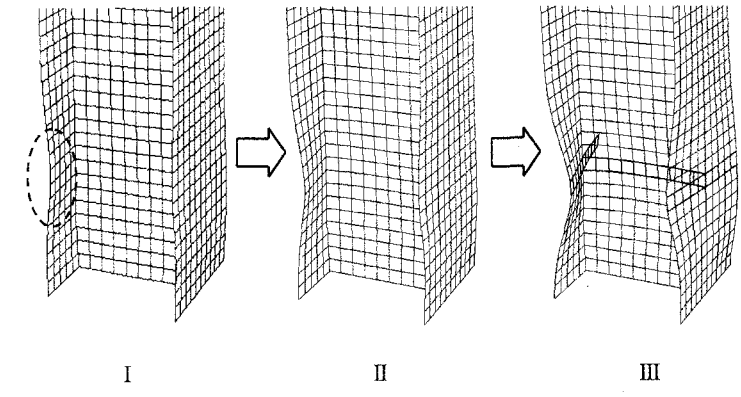

(a) Monotonic Loading

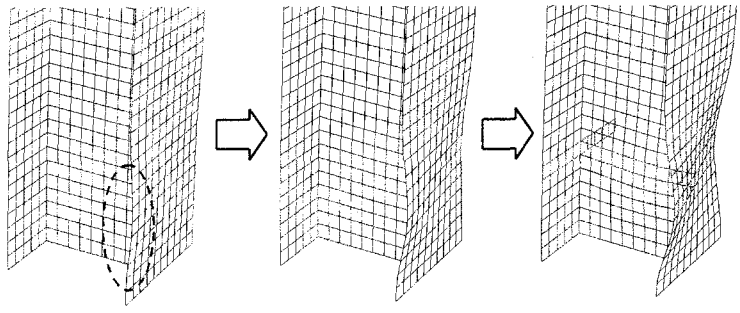

(b) Cyclic Loading

Fig. 9 Local Buckling Progress of Short Members Loaded about Strong Axis

$$R_f = \sqrt{\frac{\sigma_y}{\sigma_{cr}}} = \frac{b}{t_f}\sqrt{\frac{\sigma_y}{E}\frac{12(1-\nu^2)}{0.425\pi^2}} \quad (2)$$

$$\bar{\lambda} = \sqrt{\frac{\sigma_y}{\sigma_E}} = \frac{2h}{r}\frac{1}{\pi}\sqrt{\frac{\sigma_y}{E}} \quad (3)$$

where E: Young's modulus; σ_y: yield stress; ν: Poisson's ratio; σ_{cr}: elastic buckling stress for plate; σ_E: Euler buckling stress; b: width of half flange=B/2; k: buckling coefficient of plate=0.425 for H cross-section; r: radius of gyration of cross section.

Mild steel SS400 (defined by JIS: Japan Industrial Standards) is utilized whose nominal values of material parameters are given in Table 4. Explanation of the parameters is illustrated in the stress-strain relation in **Fig. 5**. Flange width B and cross section depth D are both equal to 400 mm and kept constant, whereas flange plate thickness t_f and column height h are varied to yield 12 cases for each loading series, with $\bar{\lambda}$ taking values from 0.2 to 0.8 and R_f from 0.40 to 0.69 respectively. Attention needs to be paid to the calculation of $\bar{\lambda}$. The same value of $\bar{\lambda}$ indicates different column heights depending on loading direction.

Cyclic horizontal loading is imposed by controlling the tip deflection of the column. The amplitude is progressively increased with an increment of yield displacement δ_y, as illustrated in **Fig. 6**. Apart from cyclic loading, monotonic loading is also conducted. Three patterns of axial force ratio P/P_y (0.20, 0.35, 0.50) are applied to each analyzed column. The column S02-40 with axial force ratio 0.20 will be denoted as S02-40-P20. Under monotonic loading cases, an ideal residual stress distribution of welding pattern was adopted (**Fig. 7**). This step is neglected under cyclic loading because it is reported that modeling of residual stresses only slightly affects the strength in the first loading loop and has little influence on the subsequent cycles[10].

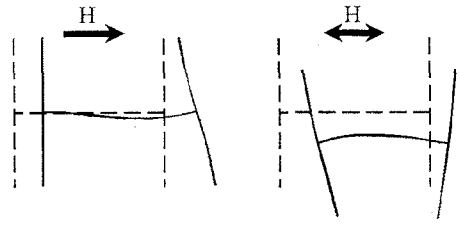

(a) Monotonic Loading **(b)** Cyclic Loading

Fig. 10 Buckled Cross Sections Loaded about Strong Axis

Following will introduce the results regarding the strong-axis and weak-axis loading separately. Prior to cyclic loading, results of monotonic loading are first explained.

(1) Failure Mechanisms of Strong-axis Loading Series

Features of the behavior are found to be closely associated with $\bar{\lambda}$, by which the columns are roughly categorized to three groups, short members ($\bar{\lambda}$ = 0.2), moderate-length members ($\bar{\lambda}$ = 0.4) and long members ($\bar{\lambda} \geq 0.6$).

a) Short Members

To explain the features of short members under monotonic loading, the horizontal load-deflection relation H-δ curve of case S02-53-P35 is given in **Fig. 8 (a)**. The horizontal axis and vertical axis on the left hand side represent the in-plane displacement δ and load H respectively, which are nondimensionalized by yielding displacement $\delta_y=(H_y h^3)/(3EI)$, and yielding load $H_y=(M_y/h)(1-P/P_y)$ accordingly. Here M_y indicates yielding moment. The vertical axis on the right hand side refers to the

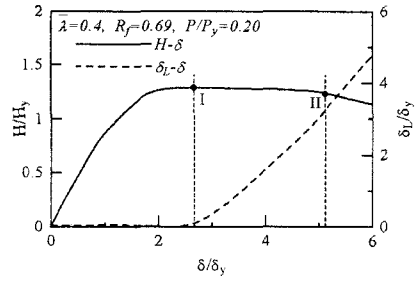

(a) Case with Low Axial Force

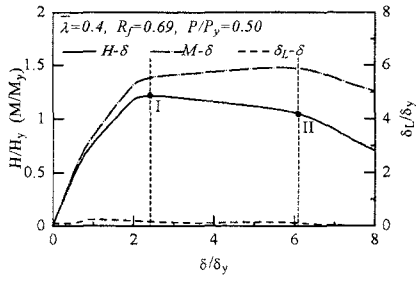

(b) Case with Higher Axial Force

Fig. 11 *H-δ* Curves for Moderate Length Members Loaded about Strong Axis Monotonically

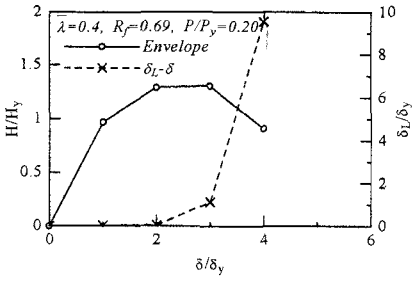

Fig. 12 Envelope of Moderate Length Members Loaded about Strong Axis Cyclically

Table 5 Summary of Strong-axis Loading Buckling Modes

$\bar{\lambda}$		0.2			0.4			0.6			0.8		
P/P_y		0.20	0.35	0.50	0.20	0.35	0.50	0.20	0.35	0.50	0.20	0.35	0.50
Loading Pattern	Monotonic	Local Buckling										Compression Buckling	
	Cyclic	Coupled Buckling			Lateral Buckling								

: Significant *P-δ* effect

out-of-plane lateral displacement δ_L divided by previously calculated δ_y. It can be seen from the figure, the lateral deflection is small enough to be negligible. The *H-δ* response indicates that the cross section was fully plasticized after yielding which increased H from H_y to near $1.3H_y$. Strain hardening was then developed and further increased H to the maximum point, before which local buckling initiated (**Fig. 9 (a)**-I) and caused H to decrease. H kept descending slowly as the buckle grew larger (**Fig. 9 (a)**-II and III) and local buckling is the cause of the failure. The *H-δ* response can be clearly divided into three parts, the elastic portion, the plastic hardening portion, and the post buckling descending portion. There is a rather long plastic hardening portion which indicates good ductility. It is also important to note the post buckling descending is not steep and can be considered for use if full using of member capacity is desired. The cross section at the mid-height of the buckle (highlighted cross section in **Fig. 9 (a)**-III) is taken out and illustrated in **Fig. 10 (a)**. It is found the deformation is unsymmetrical with respect to the vertical plane through the longitudinal axis of the column, which agrees with the configuration of first buckling mode predicted by eigenvalue analysis.

The *H-δ* hysteresis of the same case under cyclic loading is given in **Fig. 8 (b)**. Definition of the horizontal and vertical axes is the same as that under monotonic loading. The envelope curve of the hysteresis on the positive displacement side is bolded to highlight the development of peak strengths at every loop. Magnitude of lateral deflection corresponding to every loading reversal point is indicated by the dashed line. The progress of local buckling is displayed in **Fig. 9 (b)**. Though the envelope curve shows a tendency similar with that under monotonic loading, it is significant to note that under cyclic loading, lateral deflection δ_L accompanied the occurrence of local buckling. The reason for this phenomenon can be attributed to the interaction between local and lateral buckling induced by cyclic loading. Reversed and amplified horizontal loading in plastic range deteriorates the stiffness of the column more severely than that under monotonic loading, which instigates an early lateral deflection. The compressive and tensile forces which develop during the loading cycles give rise to a force component that acts perpendicularly to the flanges with inelastic curvature, and further distorts the cross section (Bertero and Popov 1965). Distortions of flanges concentrate on the concave side (**Fig. 9 (b)**) as a result of lateral deflection. The buckle develops larger, due to which the bending stiffness about the weak axis is further deteriorated, and lateral deflection accelerated. It is seen from **Fig. 8 (b)** the last loop finally broke off abruptly at a considerably smaller H compared with the previous loop. In FEM analysis, the lateral displacement diverged at this point and calculation terminated due to failure of numerical convergence. The highlighted cross section in **Fig. 9 (b)**-III is illustrated in **Fig. 10 (b)**, from which the transverse deviation of the buckled cross section can be seen. Different from observations of monotonic loading, coupled local and lateral buckling caused failure under cyclic loading. The distinction can be understood from the comparisons through **Fig. 8** to 10. It is also interesting to note the buckling configuration under cyclic loading differs from what was observed in past experimental studies. In experiments which restrained the free end to in-plane motions, interaction between lateral and local buckling was not as notable and the flanges on both sides of the web plane, in stead of only one side, were approximately equally curved.

b) Moderate-length Members

For members with moderate length, the axial force ratio P/P_y was found to have an important influence on the failure mechanism. *H-δ* response of a low axial force case S04-69-P20 is given in **Fig. 11 (a)**. Lateral deflection initiated at point I and grew notable as δ progressed. However the post-buckling strength remained quite stable until local buckling set in at point II. The dropping rate of strength was accelerated by the appearance of local buckling, which constituted the cause of the ultimate failure. A similar process was also reported by Lee and Galambos[1], in whose research a beam was bended to failure without axial force. Like short members under cyclic loading, lateral deflection is present in this case. However lateral deflection did not diverge and local buckling contributed more to the loss of strength. Based on these differences, failure of this column is attributed to local buckling.

Another example is displayed in **Fig 11 (b)** to demonstrate the influence of large axial force ($P \geq 0.35P_y$). In addition to *H-δ*

Table 6 Summary of Weak-axis Loading Buckling Modes

$\bar{\lambda}$		0.2			0.4			0.6			0.8		
P/P_y		0.20	0.35	0.50	0.20	0.35	0.50	0.20	0.35	0.50	0.20	0.35	0.50
Monotonic Loading		Local Buckling											
Cyclic Loading	R_f=0.40												
	R_f=0.53												
	R_f=0.69												

: Significant P-δ effect

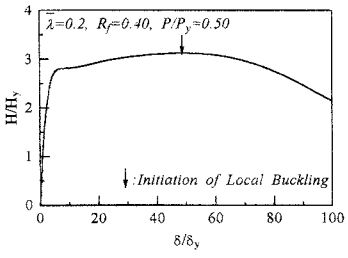

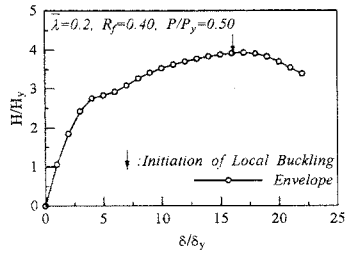

(a) Monotonic Loading **(b)** Cyclic Loading

Fig. 13 Comparison of H-δ Curves for Members Loaded about Weak Axis

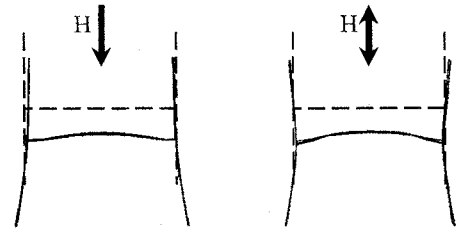

(a) Monotonic Loading **(b)** Cyclic Loading

Fig. 15 Buckled Cross Sections Loaded about Weak Axis

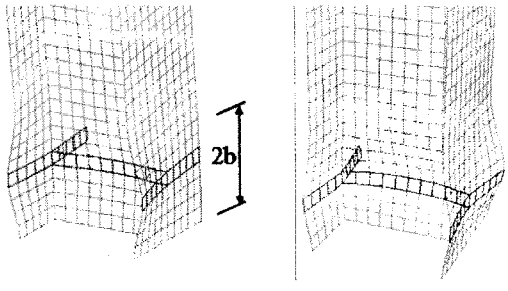

(a) Monotonic Loading **(b)** Cyclic Loading

Fig. 14 Local Buckling Configuration of Members Loaded about Weak Axis

response, total moment M ($=Hh+P\delta$) is also plotted against δ to take into consideration the contribution of P. A notable difference is that lateral deflection did not develop. The reason is attributed to P-δ effect, which amplified the total bending moment about strong axis to such an extent that the in-plane deflection tendency predominates, and lateral deflection was not triggered. From comparison between H-δ and M-δ curves, it is also found that significant P-δ effect resulted in an early drop of horizontal force H, while the overall moment bearing capacity M was still increasing as a result of the increasing contribution of P-δ effect. Local buckling arose at point II which terminated the increase of M, and caused the ultimate failure. The buckling configuration of these moderate-length members is similar with that of short members.

Cyclic loading involves a different failure mechanism. One case is given in **Fig. 12**, in which only the envelope curve of the positive displacement side of the H-δ hysteresis and the lateral deflection at reversal loading points are plotted. The general feature of the curves is similar with that of the short members, except that local buckling deformation was not observed through out the whole loading process. Lateral buckling solely caused the failure. As the in-plane cycling progressed, the free end of the column continued to deflect laterally in one direction while twisting at the same time. After the $4\delta_y$ loop, lateral distortion diverged and the column collapsed, resulting in a sudden drop of strength. For these moderate length columns, the slenderness ratio about weak axis is so large that before enough strains can localize to form a buckle, lateral buckling has already occurred and immediately leads the column to collapse.

c) Long Members

For long members, the columns undergo lateral buckling shortly after entering plastic range and experience a sudden failure. This mechanism is the same in both monotonic and cyclic loading. For cases with $\bar{\lambda} = 0.8$ and $P/P_y \geq 0.35$, applying only axial force already made the lateral deflection diverge. A check was made by calculating the weak-axis compression buckling load according to the column curves provided in ECCS recommendations[11]. The buckling load of the studied long columns was found to be in the range from $0.35P_y$ to $0.38P_y$, which is in accordance with the analytical results.

Table 4 summarizes the failure modes of all the analyzed columns subjected to horizontal loading about strong axis. Local buckling which predominates in short and moderate-length members under monotonic loading is replaced by coupled or lateral buckling under cyclic loading. This fact indicates that for structural H-section members expected to resist only static loads, their behavior can be ensured if local bucking can be avoided or delayed. However, when earthquake effect is of concern, prevention of lateral buckling will be of crucial importance. The cases for which significant P-δ effect caused early loss of horizontal resistant strength are indicated by shading.

(2) Failure Mechanisms of Weak-axis Loading Series

For columns loaded about weak axis, the failure mechanisms are greatly simplified by the absence of lateral buckling. All members loaded monotonically or cyclically, failed sooner or later due to local buckling. Buckling configurations were found to depend on loading pattern. In addition, a clearer trend of the influence of P-δ effect is observed.

a) Short Members

Beginning with short columns ($\bar{\lambda} = 0.2$ and $\bar{\lambda} = 0.4$), the H-δ responses of a typical case under monotonic loading and the envelope curve of hysteresis under cyclic loading are compared in

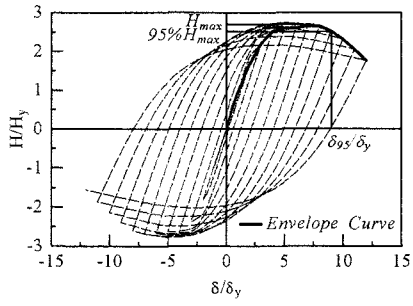

Fig. 16 Definition of Cyclic Deformation Capacity Index δ_{95}

Fig. 13. The shape of the curves exhibits similar characteristics such as plasticization of the cross section, strain hardening and a gradual drop of the strength after reaching the maximum. Sufficient plastic deformation was allowed prior to initiation of local buckling, after which the strength soon ceased to increase and deterioration commenced. The buckled shapes are compared, with the buckled segments illustrated in **Fig. 14**, and cross sections in **Fig. 15**. The length of buckled flange plates are found to be approximately $2b$ (b: width of a single flange plate = $B/2$). Buckling configuration of the column under cyclic loading differs from that under monotonic loading only in that flange plates on both sides of the web buckled symmetrically due to the cyclic effect. Local buckling is the cause of failure.

b) Long Members

The behavior is alike for longer columns ($\bar{\lambda} = 0.6$ and $\bar{\lambda} = 0.8$), except that significant P-δ effect appeared in some cases. Longer columns with higher axial force are more susceptible to significant P-δ effect. In addition, certain displacement δ that can yield a product of $P\delta$ large enough is also necessary for significant P-δ effect to occur. Thus cross sections with smaller width-to-thickness ratio parameter R_f, which indicates thicker flanges, are more possible to yield large δ prior to the occurrence of local buckling, and therefore more susceptible to P-δ effect.

Buckling modes of the analyzed columns subjected to horizontal loading about weak axis are summarized in Table 6. Local buckling is the only cause of failure. In cases of cyclic loading, columns failed at a smaller magnitude of displacement compared with monotonic loading cases. As a result cases affected by significant P-δ effect under cyclic loading were limited to only the most susceptible ones. Influence of R_f on P-δ effect is also understood.

(3) Deformation Prediction

To evaluate the deformation capacity of columns under cyclic loading, the index δ_{95}/δ_y is adopted, whose definition is illustrated in **Fig. 16**. δ_{95} corresponds to $0.95H_{max}$ on the descending portion of H-δ curve, and can account for the post-peak capacity to a certain extent. δ_{95}/δ_y of all the studied cases in this research is calculated according to this definition and is found to have a correlation with an integrated factor of dimensional and loading parameters. This correlation is plotted for strong-axis loading and weak-axis loading series respectively in **Fig. 17 (a)** and **(b)**. Through fitting of the plotted points, prediction formulas were created as expressed by Eq. 4 and 5, where S represents standard deviation of the fitting. The formulas give the mean value of the approximation of calculated results, and are designated as M curve in the figure. Though there is obvious deviation of the

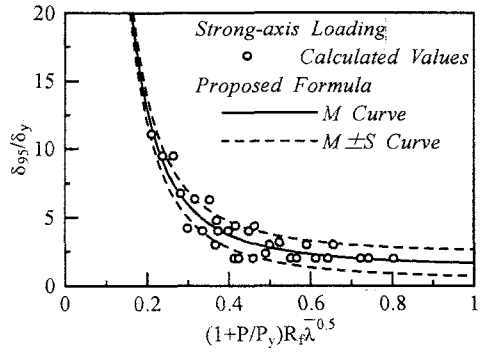

(a) Strong-axis Loading

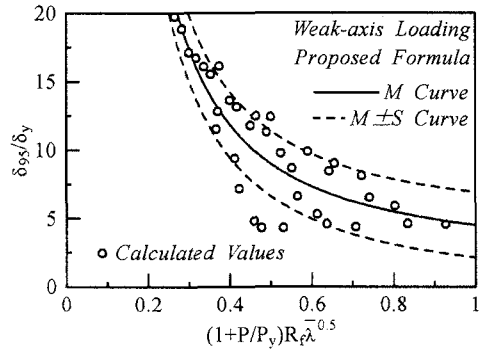

(b) Weak-axis Loading

Fig. 17 Deformation Capacity Prediction

points from the M curves, except for very few points, almost all points lie within the range of $M \pm S$.

Strong axis loading:

$$\frac{\delta_{95}}{\delta_y} = \frac{0.28}{\left[\left(1+P/P_y\right)R_f\,\bar{\lambda}^{0.5}\right]^{2.32}} + 1.39 \quad (S=0.97) \qquad (4)$$

Weak axis loading:

$$\frac{\delta_{95}}{\delta_y} = \frac{2.2}{\left[\left(1+P/P_y\right)R_f\,\bar{\lambda}^{0.5}\right]^{1.60}} + 2.32 \quad (S=2.38) \qquad (5)$$

5. Conclusions

An experimentally verified numerical model was used to study the inelastic behavior of H-section steel cantilever columns. Attention was centered on the failure mechanisms under cyclic loading, which was analyzed with respect to dimensional and loading parameters including slenderness ratio parameter $\bar{\lambda}$, width-to-thickness ratio parameter of the flange R_f and axial force ratio P/P_y. Following conclusions were obtained from the research:

(1) When load is applied about strong axis of the cross section to members with a moderate length ($\bar{\lambda} \le 0.4$), local buckling is the cause of failure under monotonic loading, whereas lateral or coupled lateral and local buckling leads to failure under cyclic loading.

(2) For members loaded about weak axis of the cross section, local buckling is the only cause of failure, disregarding the loading pattern.

(3) Horizontal resistant strength of long members with high

axial force ratio P/P_y may begin to decrease prior to buckling, due to significant P-δ effect.

(4) Equations were developed to correlate the cyclic deformation capacity δ_{95}/δ_y with parameters R_f, $\bar{\lambda}$ and P/P_y.

Acknowledgements: The experimental data used in this work was provided by Prof. I. Mitani., whose support is gratefully acknowledged by the authors.

References

1) Lee, G. C., and Galambos, T. V.: Post-buckling strength of wide-flange beams, *J. Engng Mechanics Division, ASCE*, 88(EM1), pp. 59-75, 1962.

2) Bertero, V. V., and Popov, E. P.: Effect of large alternating strains of steel beams, *J. Structural Division, ASCE*, 91(ST1), pp. 1-12, 1965.

3) Lee, G. C., and Lee E. T.: Local buckling of steel sections under cyclic loading, *J. Construct. Steel Research*, 29, pp. 55-70, 1994.

4) Yin, S., Corona, E., and Ellison, M. S.: Degradation and buckling of I-beams under cyclic pure bending, *J. Engng Mechanics, ASCE*, 130(7), pp. 809-817, 2004.

5) Vann, W. P., Thompson, L. E., Whalley, L. E., and Ozier, L. D.: Cyclic Behavior of Rolled Steel Members, *Proc. of the 5th World Conference on Earthquake Engineering*, Rome, pp. 1187-1193, 1973.

6) Suzuki, T., and Ono, T.: An experimental study on inelastic behavior of steel members subjected repeated loading, *Proc. of the 6th World Conference on Earthquake Engineering*, pp. 3163-3168, 1977.

7) Mitani, I., Makino, M., and Matsui, C.: Post local buckling behavior of steel beam-columns, Part 1: Test program and test results, *Trans. AIJ*, 281, pp. 71-80, 1979.

8) Shen, C., Mamaghani, I. H. P., Mizuno, E., and Usami, T.: Cyclic Behavior of structural steel, II: Theory, *J. Engng Mechanics, ASCE*, 121 (11), pp. 1165-1172, 1995.

9) Ge, H. B., Gao, S. B., and Usami, T.: Stiffened steel box columns, Part 1: Cyclic Behavior, *Earthquake Engng Struct. Dyn.*, 29 (11), pp. 1691-1706, 2000.

10) Banno, S., Mamaghani, I. H. P., Usami, T., and Mizuno, E.: Cyclic elasto-plastic large deflection analysis of thin steel plates, *J. Engng Mechanics, ASCE*, 124 (4), pp. 363-370, 1998.

11) Eurocode 3: Common Unified Code of Practice for Steel Structures (draft), 1983.